Void Suppression Method of CFRP Variable-Thickness Structure Components by Vibration-Assisted Curing Process

Shunming Yao , Lihua Zhan * , Chenglong Guan * , Dechao Zhang , Miaomiao Zhang

Posted Date: 7 April 2026

doi: 10.20944/preprints202604.0440.v1

Keywords: variable-thickness structure; CFRP; vibration-assisted curing process; voids suppression; out-of-autoclave

 doi:10.20944/preprints202604.0440.v1

Article

Void Suppression Method of CFRP Variable-Thickness Structure Components by Vibration-Assisted Curing Process

Shunming Yao [1], Lihua Zhan [2,*], Chenglong Guan [3,*], Dechao Zhang [2] and Miaomiao Zhang [2]

[1] College of Mechanical and Electrical Engineering, Central South University, Changsha 410083, China
[2] Light Alloys Research Institute, Central South University, Changsha 410083, China
[3] School of Mechanical Engineering and Automation, Fuzhou University, Fuzhou 350108, China
* Correspondence: yjs-cast@csu.edu.cn (L.Z.); guancl@fzu.edu.cn (C.G.)

Abstract

Composite components with variable thickness structures often suffer from insufficient forming pressure during curing due to complex pressure transfer in regions with abrupt thickness changes, which easily causes void defects and degrades component performance. In this study, a mechanical vibration-assisted double vacuum bag process is proposed. Finite element analysis of the vibration energy field in saturated porous composites is conducted, and curing experiments for variable-thickness specimens are designed. The effects of vibration, vacuum, and their synergy on void characteristics and mechanical properties are studied using microscopic characterization and mechanical tests. The results indicate that vibration can effectively facilitate gas discharge and accelerate resin flow, while the double vacuum bag process reduces gas discharge resistance in the early curing stage by delaying the vacuum negative pressure application, yet it also results in insufficient resin flow due to this delay. Through the synergistic optimization of vibration-assisted energy field parameters and the double vacuum bag process, gas-induced and flow-induced voids can be effectively suppressed while ensuring curing efficiency, reducing the macroscopic porosity of variable-thickness regions from 8.34% (single vacuum bag process) to 0.43%. This study provides a new approach for the high-quality curing and manufacturing of variable-thickness composite components.

Keywords: variable-thickness structure; CFRP; vibration-assisted curing process; voids suppression; out-of-autoclave

1. Introduction

Carbon fiber reinforced polymer (CFRP) composites have become core structural materials in high-end equipment fields such as aerospace, rail transit, and new energy equipment, owing to their outstanding properties including high specific strength, high specific modulus, excellent designability, corrosion resistance, and fatigue resistance [1,2]. To efficiently achieve the synergistic optimization of component lightweighting and load-bearing performance, variable-thickness structural designs have been widely adopted in key load-bearing components such as wing panel skins, spacecraft tank walls, and wind turbine blades. This design enables precise material placement according to load distribution, significantly improving structural efficiency and service reliability [3]. However, variable-thickness components feature large geometric fluctuations and complex ply transitions. During the curing process, the outer fibers tend to bear the majority of the forming pressure, leading to a pressure-unreachable phenomenon in the variable-thickness region. This further induces typical defects such as pores, delamination, resin-rich areas, and resin-starved areas

 doi:10.20944/preprints202604.0440.v1

[4–6]. Especially in the interlaminar transition region, the abrupt change in fiber orientation and disordered resin flow paths make it easier to form stress concentration and void aggregation [7], which severely restricts the mechanical properties and structural integrity of the components [8].

Numerous studies have confirmed that voids are one of the most critical defects affecting the performance of composite materials, which can significantly reduce interlaminar shear strength [9–11], tensile/compressive strength [12–14], flexural properties [15,16], and impact toughness [17]. In complex alternating hygrothermal environments, these voids can further accelerate performance degradation, directly threatening the service safety of equipment. Therefore, achieving low-void and high-performance curing of variable-thickness CFRP components is a key technical bottleneck to promote their large-scale application in high-end equipment.

Autoclave curing is currently the mainstream process for manufacturing high-performance composites, as it can provide stable high pressure and a uniform temperature field to effectively suppress void defects. However, with the development of components towards large-scale and integrated manufacturing, the autoclave process is limited by factors such as equipment size, high energy consumption, long cycle time, and high cost, making it difficult to meet the demand for efficient and low-cost manufacturing. In this context, out-of-autoclave (OOA) technology has emerged rapidly. With the advantages of no requirement for autoclaves, flexible manufacturing, low energy consumption, and high efficiency, it has become an important development direction for the manufacturing of large composite components [18,19]. However, OOA curing relies only on vacuum pressure for forming, which leads to problems such as insufficient pressure, inadequate resin flow, and easy blockage of gas escape channels. These issues result in high component void ratio and weak interfacial bonding. Especially in complex structural regions such as variable-thickness areas, the difficulty of defect control is significantly increased, making it hard to directly meet the requirements of high-performance components [20–24].

To break through the defect control challenge in OOA curing, scholars have carried out extensive research on directions such as prepreg system optimization [25], vacuum-assisted process improvement, and special energy field-assisted curing [26,27]. Among these, vibration-assisted curing introduces a mechanical vibration energy field, which reduces resin viscosity, enhances resin fluidity, accelerates bubble escape, and improves fiber wetting. It has a significant effect on suppressing voids and improving densification under low-pressure forming conditions [28–30]. Existing research on vibration-assisted forming mainly focuses on two directions: ultrasonic vibration and mechanical vibration. Ultrasonic vibration is mostly used in liquid forming processes such as resin transfer molding (RTM), using the cavitation effect to enhance exhaust and wetting [31,32]. Low-frequency mechanical vibration is more suitable for prepreg OOA curing systems, as it can continuously improve flow and exhaust behavior during the resin viscosity change interval, and has been proven to control component void ratio at a low level [27–30,33].

However, most existing studies analyze the influence of vibration on forming quality based on macroscopic experimental phenomena, lacking the revelation of the vibration action mechanism. A few mechanistic studies only consider vibration propagation in pure resin, ignoring the influences of time-varying viscosity of resin during curing and the saturated porous medium structure formed by fiber and resin on vibration attenuation, energy field distribution and energy transfer, making it difficult to accurately describe the distribution law of vibration inside variable-thickness components. Meanwhile, existing vibration-assisted processes are mostly applied to material pretreatment before curing, and no composite curing process based on low-frequency mechanical vibration has been reported.

Therefore, aiming at the difficulty of void control in out-of-autoclave (OOA) curing of variable-thickness CFRP components and the technical limitations of vibration-assisted and OOA curing processes, this paper proposes a novel synergistic method of vibration curing and double vacuum bag. Through finite element simulation of the vibration energy field based on the propagation characteristics of composite saturated porous media, the distribution characteristics of the vibration energy field in variable-thickness components are analyzed. Meanwhile, a multi-process comparative

 doi:10.20944/preprints202604.0440.v1

experiment of variable-thickness components is designed. Combined with metallographic characterization and interlaminar shear performance testing, the effects of vibration, double vacuum bag and their synergistic effect on void evolution, resin flow and mechanical properties are systematically revealed, and the intrinsic mechanism of void suppression in variable-thickness components by the synergistic process is clarified. Finally, low-defect and high-performance curing process of variable-thickness CFRP components is realized, providing theoretical basis and technical support for high-quality out-of-autoclave manufacturing of variable-thickness composite structures.

2. Materials and Methods

2.1. Manufacturing Method of Variable-Thickness Components

2.1.1. Materials

This study employed T800 carbon fiber/TRE231 epoxy matrix composite prepreg as the experimental material. The T800/TRE231 prepreg, with a fiber volume fraction of 58% and a resin volume fraction of 42%, was supplied by Jiangsu Changzhou Tianqi Xinxin Technology Co., Ltd., Changzhou, China. The areal density of this prepreg is 130 g/m², and the initial thickness of a single prepreg ply is 0.125 mm.

In this study, variable-thickness composite components were investigated. The variable-thickness components were fabricated using interlayer layup, as shown in Figure 1a. The thick region consisted of 22 orthogonal plies with a stacking sequence of $[0/90]_{11s}$, with dimensions of 100 × 100 mm and a total thickness of 2.75 mm. The thin region consisted of 12 orthogonal plies with a stacking sequence of $[0/90]_{6s}$, with dimensions of 100 × 100 mm and a total thickness of 1.5 mm. The overall dimension of the variable-thickness component was 200 × 100 mm. The variable-thickness region was defined as the central 10 × 100 mm area of the component, to facilitate void ratio statistics and analysis of geometric dimension changes.

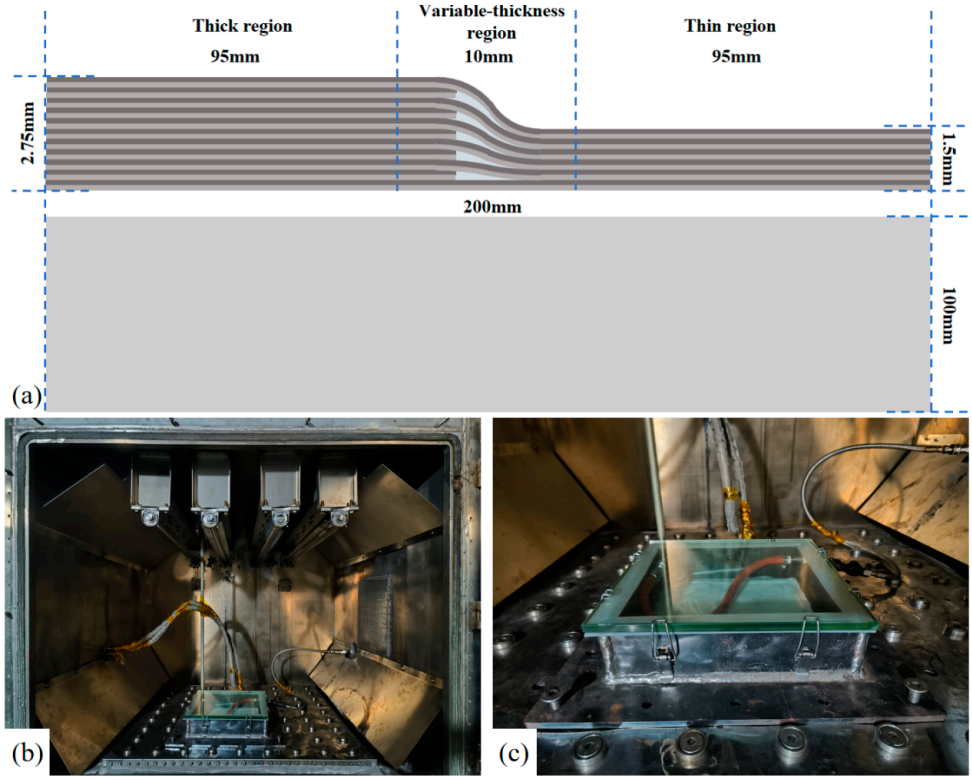

 doi:10.20944/preprints202604.0440.v1

Figure 1. Experimental preparation: (a) Schematic of layup and dimensions for the variable-thickness component; (b) Overall view of the integrated heating-vibration experimental platform; (c) Mold mounted on the vibration table.

2.1.2. Experimental Platform

Four curing forming processes were adopted in this study: the conventional vacuum bag only (VBO) process, the double vacuum bag (DVB) process, the vibration curing (VC) process, and the DVBVC synergistic process combining double vacuum bag and vibration. A self-developed integrated heating-vibration experimental platform was used in the experiments. The heating chamber provided the curing temperature, and a pneumatic vibration table installed below the chamber provided the vibration energy field required for curing forming. The pneumatic vibration table can provide broadband mechanical vibration with a frequency range of 10~5000 Hz. Two independent vacuum systems were set in the heating chamber to meet the requirements of the double vacuum bag process. The specially designed mold for the double vacuum bag process was made of 45 steel, and was mounted on the pneumatic vibration table via bolt connection, to realize the synergistic effect of the double vacuum bag process and the vibration process. The structure of the experimental platform and the mold are shown in Figure 1b and 1c.

2.1.3. Experimental Methods

The curing forming process for the variable-thickness composite components was as follows: First, the composite prepreg was laid up on the mold pre-covered with a peel ply according to the layup design. Then, according to the requirements of the VBO curing process, the peel ply, breather cloth, and vacuum bag were laid sequentially for sealing. The vacuum nozzle inside the mold cavity was installed to complete the sealing of the first vacuum bag. After ensuring good sealing inside the first vacuum bag, the transparent glass cover plate was installed on the top of the mold cavity, and the latches were locked to complete the sealing of the second vacuum chamber. After confirming the effectiveness of the two-layer vacuum sealing, the entire mold was installed on the vibration table and mounted with bolt connections. The vacuum system of the first vacuum bag and the vacuum system of the second vacuum chamber were connected separately, completing the pre-curing preparation. The schematic of related process is shown in Figure 2.

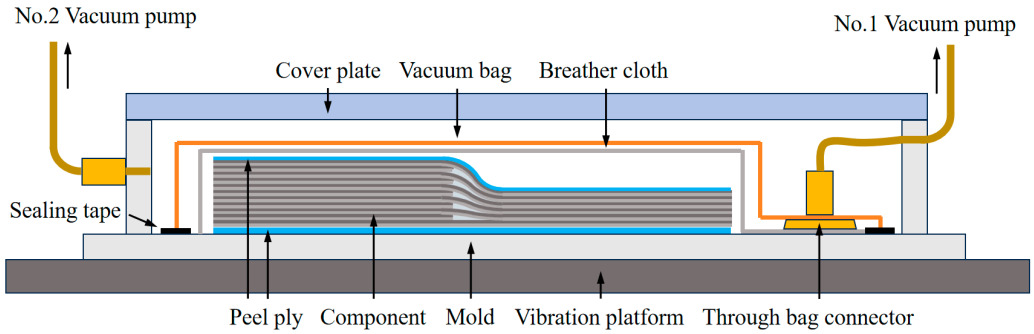

Figure 2. Schematic of the double vacuum bag vibration curing process.

After the above preparation, curing experiments were carried out according to the curing cycles of the double vacuum bag curing process, the vibration curing process, and the double vacuum bag vibration curing process, respectively. Meanwhile, the standard VBO curing process was added as the control. The curing cycles are shown in Figure 3. The heating chamber inside the pneumatic vibration table was heated and held according to the curing process requirements and then cooled to room temperature with air after the holding stage. In addition, for the double vacuum bag process, the vacuum system of the second vacuum chamber turned off the vacuum pump at the process-

 doi:10.20944/preprints202604.0440.v1

specified node and opened the vacuum pipeline to let air fully enter, ensuring that the atmospheric pressure outside the first vacuum bag generated sufficient vacuum negative pressure.

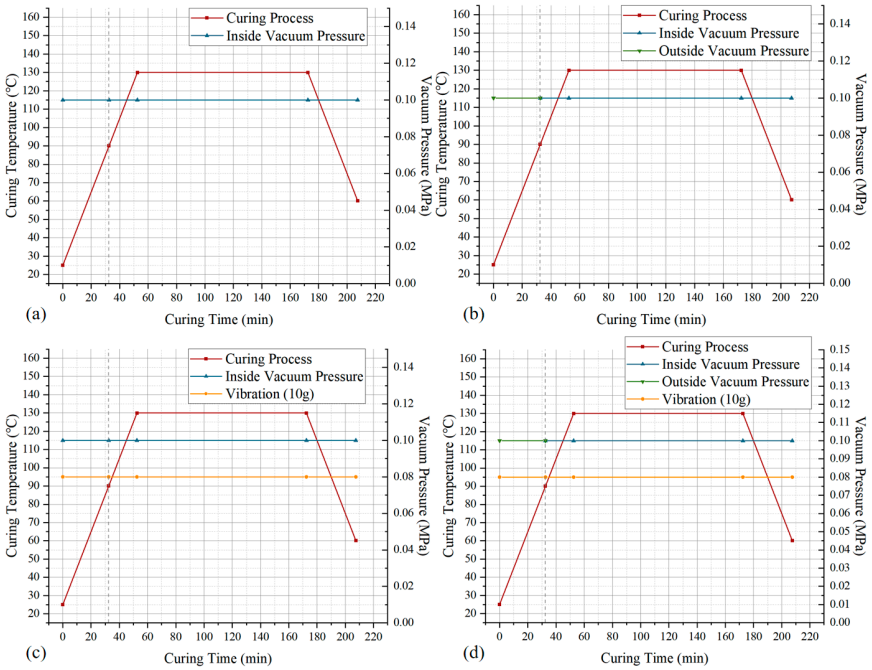

Figure 3. Curing cycles of the processes: (a) Vacuum bag only (VBO); (b) Double vacuum bag (DVB); (c) Vibration curing (VC); (d) Double vacuum bag vibration curing (DVBVC).

2.2. Characterization

2.2.1. Metallographic Characterization

To observe the changes in voids and geometric dimensions of the variable-thickness components under different processes, an optical digital microscope (ODM, model VHX-5000, KEYENCE, Osaka, Japan) was used in this study. The formed samples obtained from different curing processes were sampled at the positions shown in Figure 4. For each sample, 5 specimens were taken from the thick region, thin region, and variable-thickness region, respectively. Subsequently, these specimens were polished using waterproof abrasive papers with grit sizes of 1000, 1200, and 1500, and metallographic abrasive papers with grit sizes of 1000, 1600, and 2000. In addition, cross-sections were prepared using polishing cloth for observation with the high-depth-of-field microscope. The microscopic morphology and size distribution of the cross-sections of the specimens treated with different curing processes were carefully examined and observed. To intuitively compare the difference in void distribution in variable-thickness components under different process conditions, the void ratio of the thick region, thin region, and variable-thickness region of the samples were statistically calculated, respectively. To determine the void ratio of different curing processes and regions, Equation (1) was used:

$$\gamma = \frac{S_\gamma}{S_a} \tag{1}$$

where γ denotes the void ratio; S_γ is the area occupied by voids on the cross-section; S_a is the cross-sectional area of the specimen.

 doi:10.20944/preprints202604.0440.v1

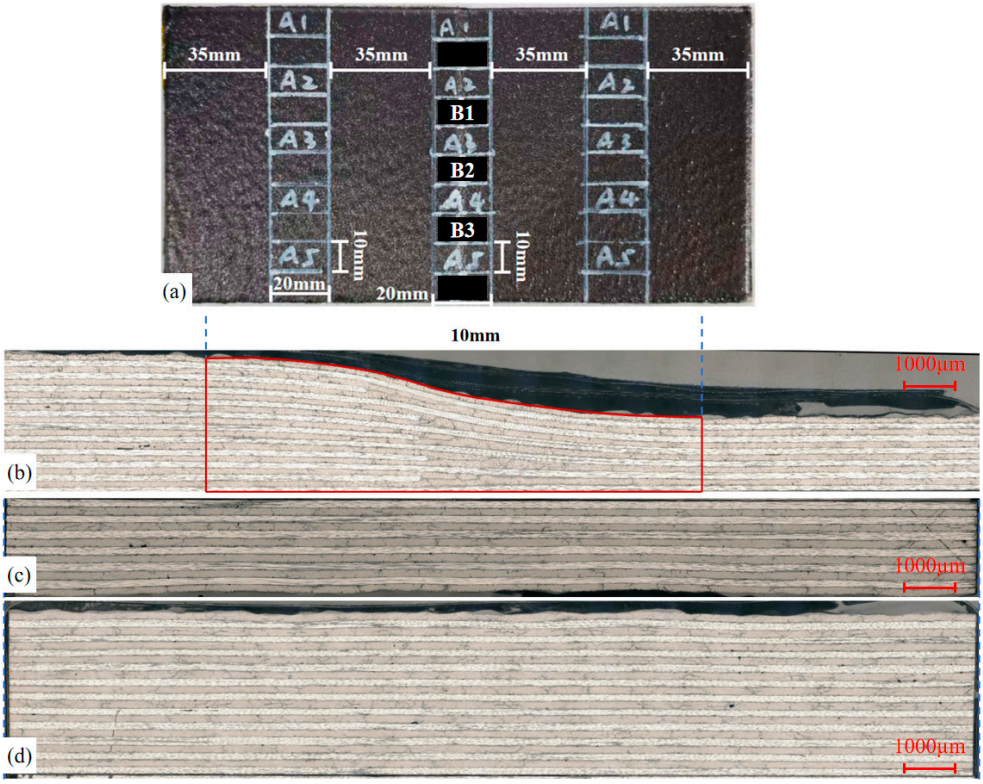

Figure 4. Microscopic observation: (a) Sampling; (b) Variable-thickness region; (c) Thin region; (d)Thick region.

In addition, to reflect the resin flow during the curing process under different processes, the geometric dimensions of the variable-thickness region after curing were statistically analyzed using the above micrographs. For the variable-thickness region, the outer contour dimensions of the corresponding region were extracted, and the projected area was calculated, as shown in Figure 4. Among them, the A-series samples were the samples for microscopic observation, and the B-series samples were the samples for mechanical property testing. All sample data were statistically analyzed to calculate the average geometric dimensions.

2.2.2. Mechanical Property Testing

Although there is no general mechanical property testing standard for variable-thickness components, this study still referred to the laminates testing method to conduct shear performance testing on the variable-thickness region of the components. This allowed horizontal comparison of the performance changes of variable-thickness components under different curing processes, and comprehensive analysis of the influence of different curing processes on the forming quality of composite materials.

To improve data accuracy, 3 specimens were selected for testing for each curing process, and the specimen dimensions are shown in Figure 5. The shear strength testing process referred to the Chinese industry standard JC/T 773—2010 for shear testing of laminates. The interlaminar shear strength was calculated using Equation (2):

$$\tau_m = \frac{2F_{max}}{b(H+h)} \tag{2}$$

where τ_m is the interlaminar shear strength; F_{max} is the maximum load; b is the width of the specimen, and H, h are the thick region and thin region thickness of the specimen, respectively.

 doi:10.20944/preprints202604.0440.v1

Figure 5 shows the short-beam three-point bending testing process for the variable-thickness specimens. A CMT5105 electronic universal testing machine (SANS Testing Machine Co., Ltd., Zhuhai, Guangdong, China) with a force range of 5~10 t was used as the experimental equipment. After the indenter initially contacted the surface of the composite specimen, the indenter pressed down at a rate of 1 mm/min until delamination failure occurred in the composite.

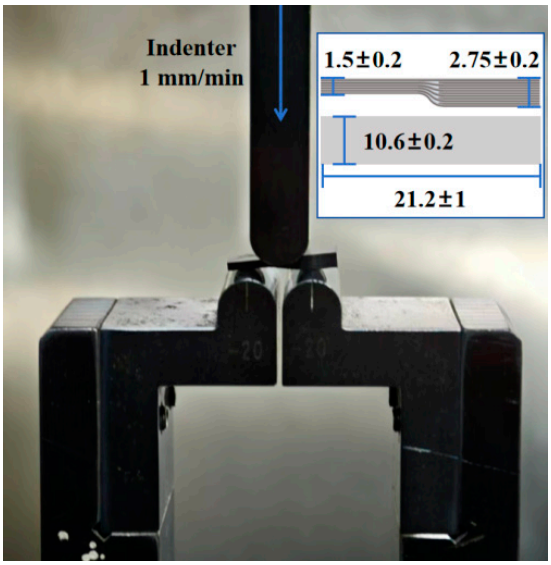

Figure 5. The short-beam three-point bending testing.

3. Finite Element Analysis

In this study, combined with Biot's theory of saturated porous media and the orthotropic constitutive relation of composite materials [34–36], the wave equation for orthotropic composite saturated porous media was established:

$$
\begin{cases}
\rho\dfrac{\partial^2 u_{x_1}}{\partial t^2}+\rho_f\dfrac{\partial^2 W_{x_1}}{\partial t^2}=A_{11}\dfrac{\partial^2 u_{x_1}}{\partial x_1^2}+A_{12}\dfrac{\partial^2 u_{x_2}}{\partial x_1\partial x_2}+A_{13}\dfrac{\partial^2 u_{x_3}}{\partial x_1\partial x_3}+\dfrac{M_1}{M}\left(\dfrac{\partial p_w}{\partial x_1}-M_1\dfrac{\partial^2 u_{x_1}}{\partial x_1^2}-M_2\dfrac{\partial^2 u_{x_2}}{\partial x_1\partial x_2}-M_3\dfrac{\partial^2 u_{x_3}}{\partial x_1\partial x_3}\right)\\
\qquad +2A_{66}\left(\dfrac{\partial^2 u_{x_2}}{\partial x_1\partial x_2}+\dfrac{\partial^2 u_{x_1}}{\partial x_2^2}\right)+2A_{55}\left(\dfrac{\partial^2 u_{x_3}}{\partial x_1\partial x_3}+\dfrac{\partial^2 u_{x_1}}{\partial x_3^2}\right)\\
\rho\dfrac{\partial^2 u_{x_2}}{\partial t^2}+\rho_f\dfrac{\partial^2 W_{x_2}}{\partial t^2}=A_{12}\dfrac{\partial^2 u_{x_1}}{\partial x_1\partial x_2}+A_{22}\dfrac{\partial^2 u_{x_2}}{\partial x_2^2}+A_{23}\dfrac{\partial^2 u_{x_3}}{\partial x_2\partial x_3}+\dfrac{M_2}{M}\left(\dfrac{\partial p_w}{\partial x_2}-M_1\dfrac{\partial^2 u_{x_1}}{\partial x_1\partial x_2}-M_2\dfrac{\partial^2 u_{x_2}}{\partial x_2^2}-M_3\dfrac{\partial^2 u_{x_3}}{\partial x_2\partial x_3}\right)\\
\qquad +2A_{66}\left(\dfrac{\partial^2 u_{x_2}}{\partial x_1^2}+\dfrac{\partial^2 u_{x_1}}{\partial x_1\partial x_2}\right)+2A_{44}\left(\dfrac{\partial^2 u_{x_2}}{\partial x_2\partial x_3}+\dfrac{\partial^2 u_{x_3}}{\partial x_3^2}\right)\\
\rho\dfrac{\partial^2 u_{x_3}}{\partial t^2}+\rho_f\dfrac{\partial^2 W_{x_3}}{\partial t^2}=A_{13}\dfrac{\partial^2 u_{x_1}}{\partial x_1\partial x_3}+A_{23}\dfrac{\partial^2 u_{x_2}}{\partial x_2\partial x_3}+A_{33}\dfrac{\partial^2 u_{x_3}}{\partial x_3^2}+\dfrac{M_3}{M}\left(\dfrac{\partial p_w}{\partial x_3}-M_1\dfrac{\partial^2 u_{x_1}}{\partial x_1\partial x_3}-M_2\dfrac{\partial^2 u_{x_2}}{\partial x_2\partial x_3}-M_3\dfrac{\partial^2 u_{x_3}}{\partial x_3^2}\right)\\
\qquad +2A_{55}\left(\dfrac{\partial^2 u_{x_3}}{\partial x_1^2}+\dfrac{\partial^2 u_{x_1}}{\partial x_1\partial x_3}\right)+2A_{44}\left(\dfrac{\partial^2 u_{x_2}}{\partial x_2\partial x_3}+\dfrac{\partial^2 u_{x_3}}{\partial x_2^2}\right)\\
-\dfrac{\partial p_w}{\partial x_1}=\rho_f\dfrac{\partial^2 u_{x_1}}{\partial t^2}+m_1\dfrac{\partial^2 W_{x_1}}{\partial t^2}+r_1\dfrac{\partial W_{x_1}}{\partial t}\\
-\dfrac{\partial p_w}{\partial x_2}=\rho_f\dfrac{\partial^2 u_{x_2}}{\partial t^2}+m_2\dfrac{\partial^2 W_{x_2}}{\partial t^2}+r_2\dfrac{\partial W_{x_2}}{\partial t}\\
-\dfrac{\partial p_w}{\partial x_3}=\rho_f\dfrac{\partial^2 u_{x_3}}{\partial t^2}+m_3\dfrac{\partial^2 W_{x_3}}{\partial t^2}+r_3\dfrac{\partial W_{x_3}}{\partial t}
\end{cases}
\tag{3}
$$

 doi:10.20944/preprints202604.0440.v1

where σ_{x_i} and $\tau_{x_i x_j}$ are the stress components of the solid skeleton; p_w is the pore pressure of the saturated fluid; A_{11}, A_{12}, A_{13}, A_{22}, A_{23}, A_{33}, A_{44}, A_{55}, A_{66}, M_1, M_2, M_3, M corresponds to the 13 independent elastic parameters associated with the properties of the solid framework and pore fluid in orthotropic porous media; where $W_{x_i} = \phi(U_i - u_i)$ is the displacement of the pore fluid relative to the solid framework, ϕ is the porosity, U_i is the displacement of the pore fluid, and u_i is the displacement of the solid framework, $i, j = 1,2,3$; $\rho = (1-\phi)\rho_s + \phi\rho_f$ represents the average density of the two-phase medium, ρ_s represents the density of the solid framework, ρ_f represents the density of the pore fluid; $m_j, r_j\ (j = 1,2,3)$ represent the Biot dissipation coefficient. These variables are functions of the wave frequency and can be expressed by Equation (4):

$$\begin{cases} m_j = \dfrac{\rho_f}{\phi}\alpha_j(\omega) \\ r_j = \dfrac{\eta_w}{K_j(\omega)} \\ \alpha_j(\omega) = \dfrac{\mathrm{i}\eta_w\phi}{K_j(\omega)\omega\rho_f} \\ K_j(\omega) = \dfrac{k_0}{\left\{1 - \dfrac{4\mathrm{i}\alpha_\infty^2 k_0^2 \rho_f \omega}{\eta_w \Lambda^2 \phi^2}\right\}^{\frac{1}{2}} - \dfrac{\mathrm{i}\alpha_\infty k_0 \rho_f \omega}{\eta_w \phi}} \end{cases} \tag{4}$$

where i represents the imaginary unit, $\alpha_j(\omega)$ represents the dynamic pore curvature, $K_j(\omega)$ represents the dynamic permeability, η_w represents the dynamic viscosity coefficient (dynamic viscosity), α_∞ represents the dynamic pore curvature at infinite frequency (equivalent to the tortuosity factor τ discussed below), k_0 represents the permeability at $\omega = 0$, and Λ represents the characteristic pore size.

Based on the above theoretical model, this study used COMSOL Multiphysics simulation software to analyze the vibration propagation during the curing process of fiber-reinforced composite preforms. The material parameters required for the analysis are shown in Table 1.

Table 1. Properties of the composite preform.

Porous parameters	
Permeability, $S_{11} = S_{22}$	6.72×10^{-13}
Permeability, S_{33}	1.72×10^{-14}
Tortuosity factor, $\tau_{11} = \tau_{22}$	5.1
Tortuosity factor, τ_{33}	7.97
Mechanical properties	
Young's modulus, $E_{11} = E_{22}$/GPa	100.43
Young's modulus, E_{33}/GPa	9.75
Shear modulus, $G_{12} = G_{13}$/GPa	7.15
Shear modulus, G_{23}/GPa	4.55
Poisson's ratio, $\nu_{12} = \nu_{13}$	0.315

 doi:10.20944/preprints202604.0440.v1

Poisson's ratio, ν_{23}	0.07
Fluid properties	
Viscosity μ_r / Pa·s	1
Density / kg·m^{-3}	1200

To accurately reflect the characteristics of the variable-thickness structure, a geometric model of the variable-thickness laminate preform with dimensions of 200 × 100 mm (length × width) and layup referring to the experimental design was established. A 10 mm perfectly matched layer (PML) was set on the outer layer to prevent the echo generated by the hard boundary from affecting the model analysis, as shown in Figure 6a. For meshing, free tetrahedral mesh was used for the component grid elements, as shown in Figure 6b, and automatic swept mesh was used for the PML layer, as shown in Figure 6c. According to the vibration frequency range of the pneumatic vibration table, the sweep frequency range of the model was set to 1 to 5001 Hz, with a sweep interval of 50 Hz.

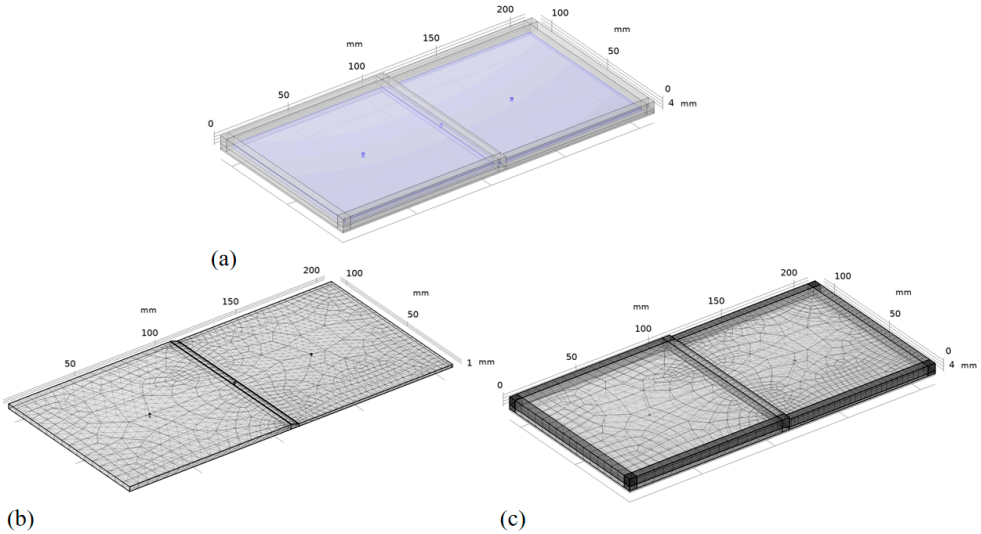

Figure 6. Finite element analysis of the vibration propagation process: (a) Geometric model of the variable-thickness component; (b) Mesh division of the component; (c) Mesh division of the PML.

To realize the vibration propagation analysis under the process conditions of the vibration table, a zero-phase Ricker wavelet was used as the vibration excitation to investigate the vibration response in the frequency domain. The expression of the Ricker wavelet in the frequency domain is as follows:

$$R(f) = \frac{2f^2}{\sqrt{\pi} f_{main}^3} e^{-\frac{f^2}{f_{main}^2}} e^{-j2\pi f} \tag{5}$$

where f_0 is the dominant frequency of the Ricker wavelet.

Referring to the spectrum range of Ricker wavelets with different dominant frequencies, a Ricker wavelet with a dominant frequency of 1000 Hz was selected as the vibration excitation for analysis. The vibration excitation was applied in three forms: the entire bottom surface, the thick and thin regions of the bottom surface, and the variable-thickness region of the bottom surface. The center points at the half-length position of the thick region, thin region, and variable-thickness region of the component were taken as the monitoring points for response data, to analyze the changes in the response spectrum, as shown in Figure 7.

 doi:10.20944/preprints202604.0440.v1

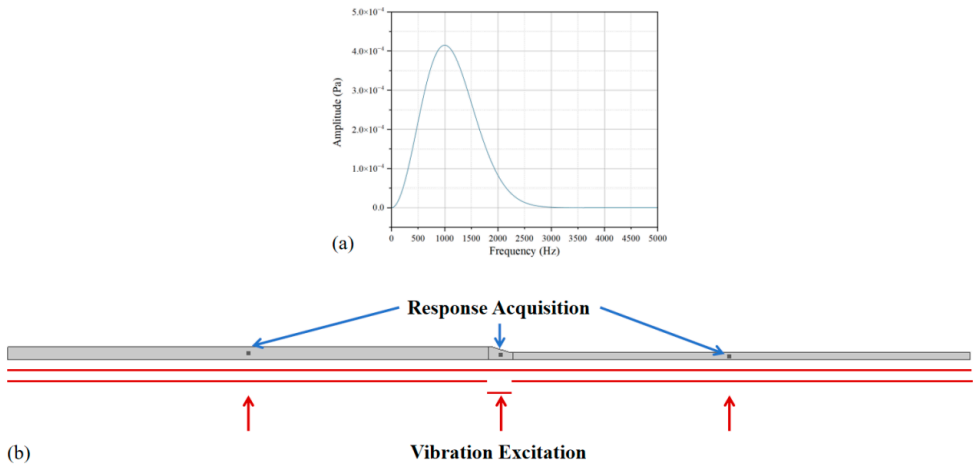

Figure 7. Ricker wavelet analysis: (a) Spectrum of the 1000 Hz dominant frequency; (b) Vibration excitation and response acquisition.

4. Results and Discussion

4.1. Influence of Vibration

In OOA processes, due to the lack of a high-pressure forming environment, the forming of components relies on vacuum pressure difference to realize the discharge of gas within and between plies. Then, by increasing the curing temperature, the resin viscosity is reduced, promoting resin flow to wet the emptied channel pores, and finally achieving densification. According to this process characteristic, the void formation mechanisms in OOA processes can be mainly divided into two categories: gas-induced and flow-induced. Gas-induced voids are formed by the residual air trapped inside the composite preform and the volatiles of the resin that cannot be completely discharged, which mostly occur during the pretreatment stages such as layup and the early curing stage when the resin viscosity is high. Flow-induced voids are mainly formed during the process of resin flow wetting the exhaust channels, where uneven resin flow or insufficient wetting leaves cavities after resin gelation. These mostly occur in the middle and later stages when the resin viscosity rises rapidly. Meanwhile, insufficient resin flow and wetting will also affect the interfacial properties of the composite materials.

Mechanical vibration has been proven to have a significant effect on suppressing voids during composite curing. From the perspective of the OOA curing process, for gas-induced voids, mechanical vibration can enhance the dynamic pressure fluctuation of the resin inside the composite, accelerate the gas diffusion process, and promote the escape of trapped gas and volatiles. For flow-induced voids, vibration can improve the uniformity of resin distribution by enhancing resin fluidity, reducing voids caused by local wetting lag. Meanwhile, it accelerates the wetting process of resin on fiber bundles at the mesoscale. Especially in the variable-thickness region, it avoids void formation by improving the resin fluidity in the complex structural region.

Therefore, the distribution of the vibration energy field in the variable-thickness component determines the magnitude of the vibration effect on different regions. Figure 8a shows the sound pressure response of the variable-thickness component under the excitation of the Ricker wavelet on the entire bottom surface. It can be seen that in the middle layer of the component, the sound pressure amplitude of the vibration response in the thick region and thin region is about 40% of the excitation signal amplitude, while that in the variable-thickness region is about 70% of the excitation signal amplitude. Separate analysis of the response sound pressure distribution under the vibration excitation of the thick and thin regions shows that the vibrations of the two regions have a superposition gain in the variable-thickness region, as shown in Figure 8b. Separate analysis of the response sound pressure distribution under the vibration excitation of the variable-thickness region

 doi:10.20944/preprints202604.0440.v1

shows that the response in the variable-thickness region is similar to the response in the thick and thin regions under the overall excitation, as shown in Figure 8c. Therefore, it can be seen that the vibration response in the variable-thickness region is subject to a greater effect from the vibration energy field, due to the gain from the thick and thin regions.

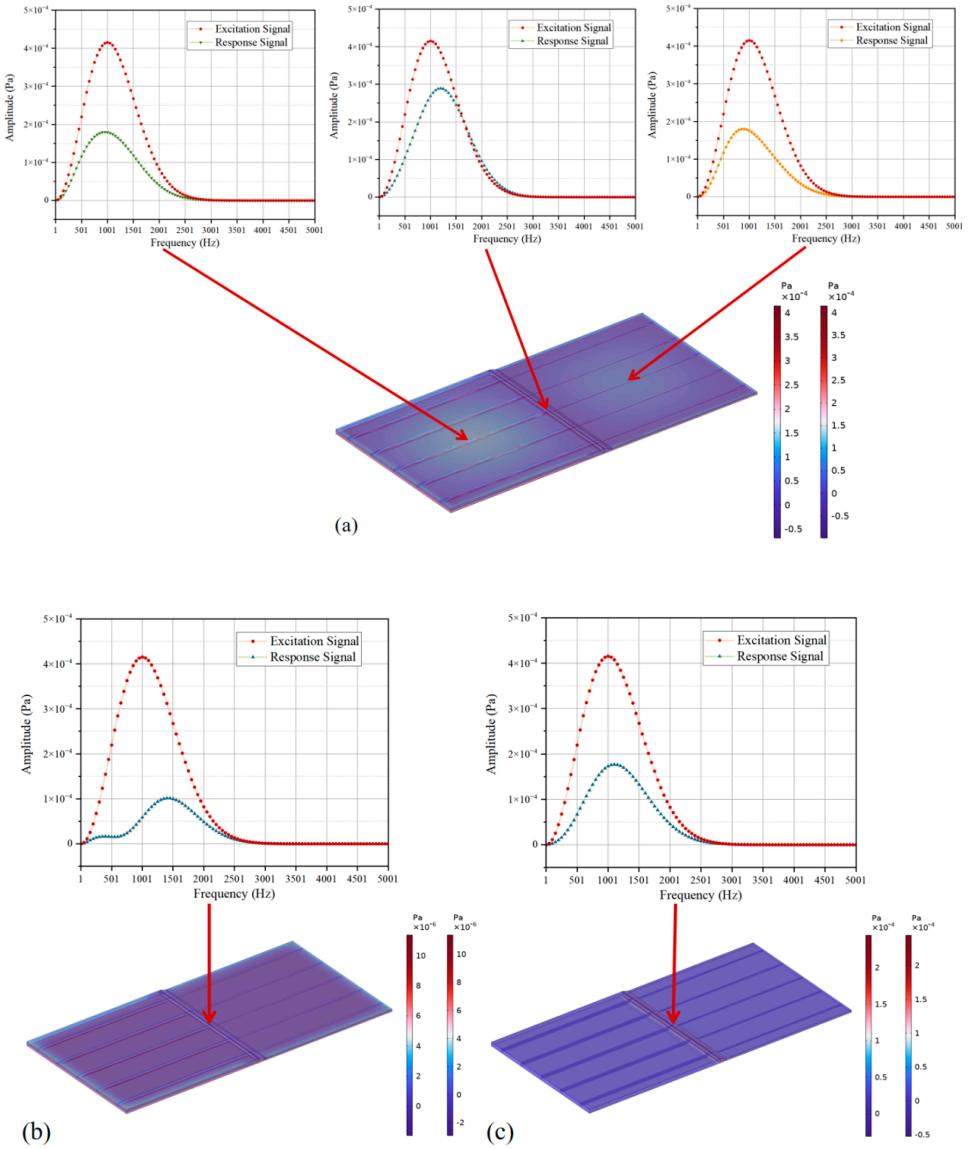

Figure 8. Ricker wavelet analysis: (a) Entire bottom surface excitation; (b) the thick and thin regions of the bottom surface excitation; (c) the variable-thickness region of the bottom surface excitation.

However, the influence of vibration on void behavior is not a simple linear relationship. Figure 9 shows the comparison of void ratio in different regions form different processes. It can be seen that the void ratio of the VBO process in the variable-thickness region is significantly higher than that in the thin and thick regions. This is because the interlaminar hybrid structure in the variable-thickness region is complex, and the paths for gas permeation and resin flow are complicated, leading to more closed bubbles generated by trapped gas and entrained bubbles generated by unbalanced resin wetting. Vibration can effectively improve gas escape and resin wetting, thereby suppressing void formation. In terms of void ratio, the void ratio of the vibration process is much lower than that of the VBO process, and the difference in void ratio between the variable-thickness region and the thick/thin regions is smaller, proving the positive effect of vibration.

 doi:10.20944/preprints202604.0440.v1

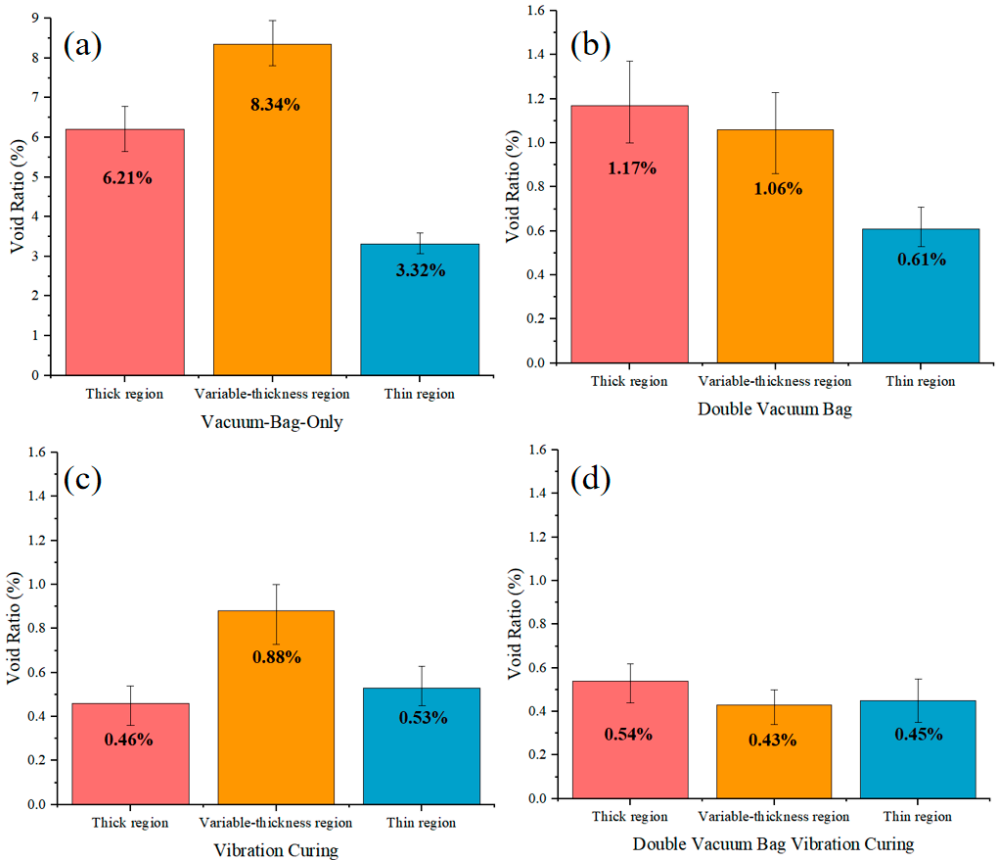

Figure 9. Comparison of void ratio: (a) Vacuum bag only (VBO); (b) Double vacuum bag (DVB); (c) Vibration curing (VC); (d) Double vacuum bag vibration curing (DVBVC).

However, comparing the absolute values of void ratio in different regions, the gap between the void ratio of the thin region, variable-thickness region (which were greatly affected by vibration in the simulation analysis), and thick region is reduced. This indicates that as the absolute number of bubbles decreases, the influence of vibration on voids has a marginal effect. Therefore, for the vibration process, it can be considered that under the condition of sufficient vibration action time, the influence of the difference in vibration energy field distribution will be reduced due to the marginal effect.

 doi:10.20944/preprints202604.0440.v1

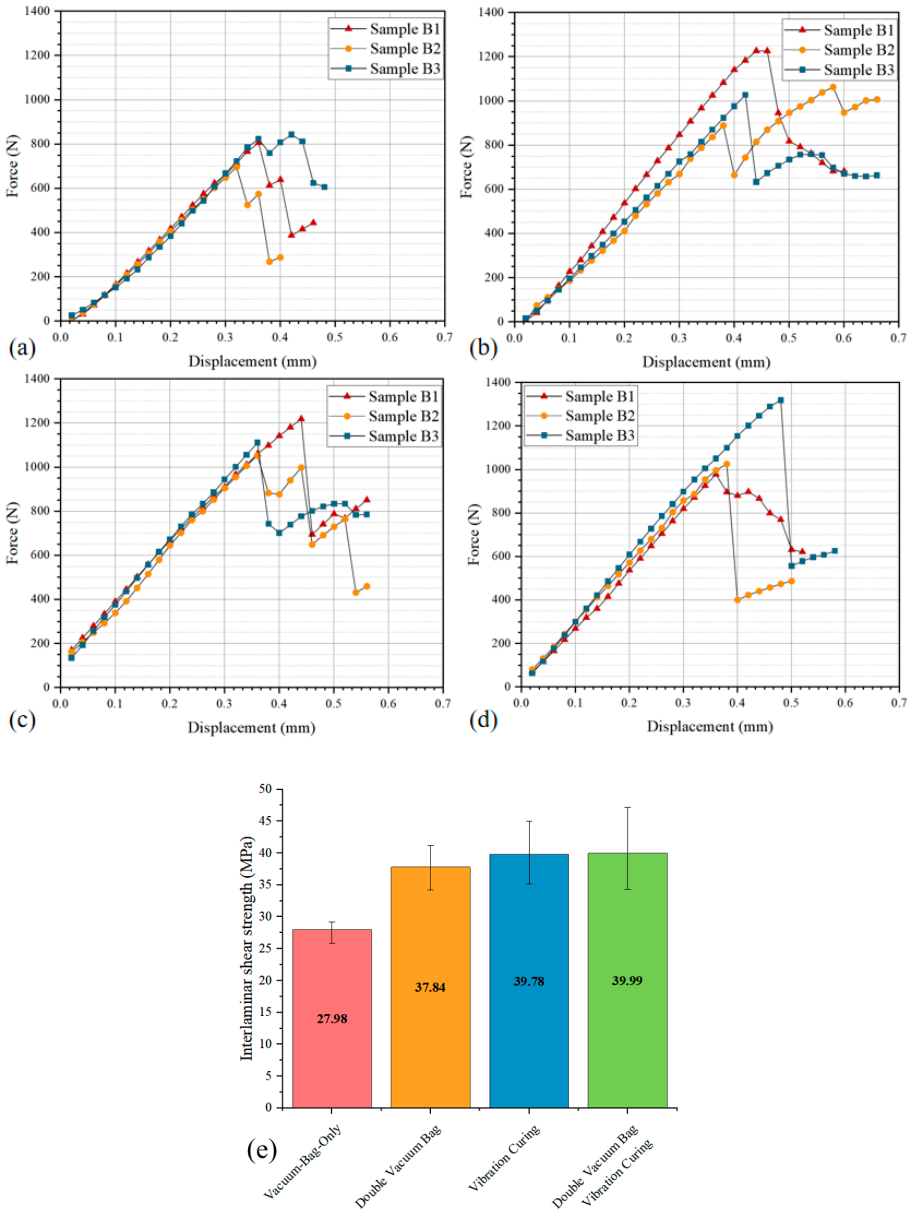

Figure 10. Comparison of interlaminar shear properties: (a) Force–displacement curve of VBO; (b) Force–displacement curve of DVB; (c) Force–displacement curve of VC; (d) Force–displacement curve of DVBVC; (e) Results of interlaminar shear strength under different processes.

In addition, the differences in interlaminar shear strength and geometric dimensions between the VBO process and the vibration process also illustrate the positive effect of vibration on the interfacial properties of the variable-thickness region. It can be seen that the interlaminar shear strength of the VBO process is about 60% of that of the vibration process. This proves that vibration not only effectively suppresses void formation but also promotes the sufficient flow of resin in the variable-thickness region and the sufficient wetting with fiber bundles, thereby improving the interfacial properties of the variable-thickness region. Meanwhile, the projected area of the variable-thickness region in the vibration process is smaller, proving that vibration has a positive promoting effect on the resin flow of the entire variable-thickness component.

 doi:10.20944/preprints202604.0440.v1

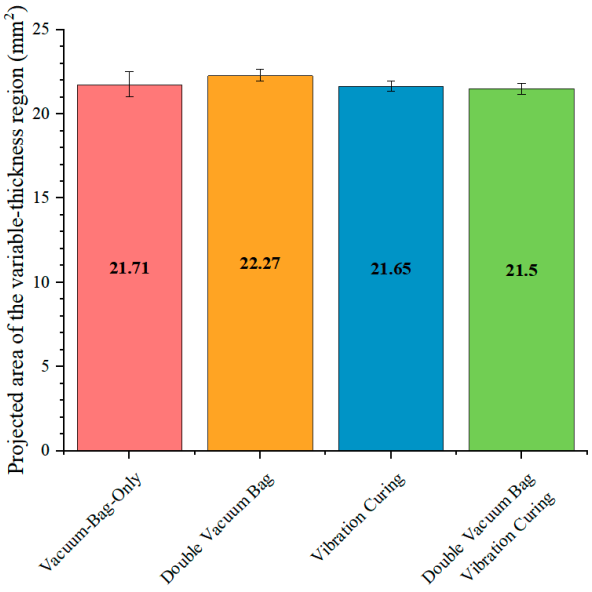

Figure 11. Comparison of projected area.

Similarly, the difference in the projected area of the variable-thickness region between the vibration process and the VBO process is small, which proves that the influence of vibration on resin flow also has a marginal effect. This may be due to the increase in the fiber volume fraction and the dynamic permeability of the porous medium after the resin gradually flows out.

4.2. Influence of Vacuum

In the VBO process, the vacuum environment inside the vacuum bag provides the driving force for gas discharge, and the vacuum bag film applies uniform pressure on the resin to promote its flow and wetting, which correspond to the formation mechanisms of gas-induced and flow-induced voids, respectively. However, in the VBO process, to apply the vacuum environment, it is necessary to seal the component with a vacuum bag film. During the discharge of gas-induced voids, the pressure from the vacuum bag film does not accelerate the discharge of air. On the contrary, it compresses the preform, leading to the compression or even closure of open pores, inhibiting the ballooning effect of gas-containing voids under negative pressure, thereby hindering the smooth escape of internal gas. Therefore, to avoid the blockage of exhaust channels caused by premature application of vacuum pressure, the VBO process usually adds a pre-treatment vacuum pumping stage before curing heating, to conduct initial vacuum pumping when the resin viscosity has not yet decreased, increasing the time window for gas discharge. However, for variable-thickness components, due to the complex structure of the variable-thickness region, there are large gaps between the fiber layers after layup, which are also filled with air. The pre-vacuum process can hardly completely avoid the premature compression of the preform by the vacuum bag pressure. After compression, more gas is trapped in the variable-thickness region, leading to larger residual voids.

To avoid the influence of vacuum bag pressure on gas escape, the double vacuum bag process was proposed, as shown in Figure 2. At the beginning of the process, the vacuum pumps for the inner and outer chambers were started simultaneously, so that while the inner chamber formed a vacuum environment, the vacuum bag film did not exert negative pressure on the preform. Then, the temperature was raised to 90 °C, where the resin viscosity decreased to a low value. At this point, the vacuum pump for the outer chamber was turned off and connected to the atmospheric environment, so that the inner vacuum bag generated negative pressure. The temperature was held for 30 min to allow sufficient resin flow. Finally, the curing temperature was raised to 130 °C, and held for 2 h to complete the curing forming. The double vacuum bag process effectively decoupled the gas-induced

 doi:10.20944/preprints202604.0440.v1

stage and the flow-induced stage, realizing the control of the pressing timing in the variable-thickness region, and ensuring smooth exhaust during the gas-induced stage.

As shown in Figure 9, the void ratio of the DBO process is significantly lower than that of the VBO process. Especially in the variable-thickness region, there is small difference in void ratio compared with the thin and thick regions. This proves that the DBO process can effectively alleviate the problem of exhaust channel collapse caused by the compression of the single-layer film in the traditional VBO process. It not only ensures the smooth escape of gas in the early stage, but also applies pressure in time during the flow stage to promote wetting. Especially, it improves the filling consistency of the variable-thickness region, greatly reducing the void ratio.

However, in the DBO process, the action time of vacuum pressure is shorter than the curing cycle, which limits the time window for resin flow and wetting. Meanwhile, it also affects the formation time of the microscopic interface between resin and fibers, thereby weakening the interfacial bonding strength. Comparing the interlaminar shear properties of the vibration curing process and the DBO process, it can be seen that although the DBO process can also significantly reduce void ratio, its interlaminar shear strength is lower than that of the components fabricated by the vibration process with similar void ratio. Meanwhile, the geometric dimensions are larger, indicating insufficient resin flow and problems in interfacial bonding performance in the DBO process. Therefore, to maintain the advantage of the DBO process in gas-induced void control, while compensating for its shortcomings in resin flow regulation and interface formation, it is necessary to introduce a new mechanism that neither interferes with the rapid discharge of air during the gas-induced stage, nor actively regulates the resin wetting behavior.

4.3. I Synergistic Influence of Vibration and Vacuum

From the characteristics of the vibration-assisted curing process and the double vacuum bag process mentioned above, it can be seen that the vibration curing process can effectively improve the resin fluidity and wettability during the flow-induced stage, while the double vacuum bag process can effectively ensure smooth exhaust during the gas-induced stage, especially avoiding the collapse of gas escape channels caused by single-layer film compression in the variable-thickness region. Combining the vibration-assisted process and the double vacuum bag process can take advantage of both processes: During the gas-induced stage, since the negative pressure generated by the vacuum bag film has not been applied, vibration not only does not interfere with the gas escape channels inside the preform, but also promotes the rapid migration of gas along low-resistance paths in the vacuum environment, enhancing the initial exhaust efficiency. After entering the flow-induced stage, the synergistic effect of vibration and the negative pressure applied by the vacuum bag film can compensate for the problems of resin fluidity and wettability in the DBO process, suppress flow-induced voids, and improve interfacial properties at the same time.

As shown in Figure 9,10 and 11, the void ratio, interlaminar shear properties, and projected area of the double vacuum-vibration synergistic process are presented. It can be seen that the void ratio of the synergistic process is further reduced compared with the DBO process and the vibration process, and the void ratio in the variable-thickness region is basically consistent with that in the thin and thick regions. This indicates that the synergistic effect of vibration and vacuum not only effectively suppresses the formation of both gas-induced and flow-induced voids, but also significantly improves the wetting uniformity of resin in complex structural regions. Comparing the interlaminar shear properties, it can be seen that the interlaminar shear strength of the synergistic process is increased by about 100% compared with the VBO process, and also has a certain improvement compared with the vibration process, with significantly improved interlaminar bonding quality.

The above results indicate that the synergistic effect of vibration and vacuum not only effectively suppresses dual gas-induced and flow-induced voids, but also promotes sufficient resin wetting and interfacial densification, realizing the synergistic optimization of low void ratio and high interfacial

 doi:10.20944/preprints202604.0440.v1

performance. This provides a new approach for the high-quality forming of complex-structure composite materials.

5. Conclusions

In this paper, by combining the vibration-assisted curing process and the double vacuum bag process, the curing void defects in variable-thickness CFRP components were effectively suppressed. Through designing curing process experiments for variable-thickness components, combined with metallographic characterization, mechanical property testing, and finite element analysis of vibration energy fields based on the propagation characteristics of composite saturated porous media, the influence of vibration, vacuum, and their synergistic effect on void defects and mechanical properties of composite materials was studied. The specific conclusions are as follows:

Based on the vibration propagation model of composite porous media, the propagation law of the vibration energy field inside the variable-thickness composite component was simulated and analyzed. Combined with the curing process experiments of variable-thickness composite components, it was proved that compared with the VBO process, the vibration process has a significant void suppression effect, while improving the resin flow and wetting uniformity in the variable-thickness region, and enhancing the interfacial bonding performance.

Based on the experimental results of double vacuum bag curing, the void evolution characteristics of the variable-thickness structure were analyzed. It proved the negative influence of vacuum negative pressure on gas-induced voids, especially in the variable-thickness region. It verified the advantage of the double vacuum bag process in suppressing gas-induced voids in the variable-thickness region, and also identified the limitations of the double vacuum bag process in terms of resin fluidity and wettability.

Based on the characteristics of the vibration process and the double vacuum bag process, a double vacuum bag-vibration synergistic curing process was proposed. The curing process experiment results show that compared with the vibration process and the double vacuum bag process, the synergistic process further reduces the void ratio and improves the interlaminar shear performance, realizing the improvement of the curing forming quality of variable-thickness components. This provides a new idea for the curing forming process of complex-structure composite components.

Author Contributions: Writing – original draft, Shunming Yao; Validation, Shunming Yao and Lihua Zhan; Software, Shunming Yao and Miaomiao Zhang; Methodology, Shunming Yao and Miaomiao Zhang; Investigation, Shunming Yao, Chenglong Guan and Dechao Zhang; Resources: Lihua Zhan; Funding acquisition, Lihua Zhan and Chenglong Guan; Conceptualization, Lihua Zhan; Writing – review & editing, Chenglong Guan and Dechao Zhang; Data curation, Chenglong Guan.

Funding: This work was fund by National Natural Science Foundation of China (52175373), National Key Research and Development Program of China (2024YFB3411102), Natural Science Foundation of Fujian Province (2024J01240), and Open Research Fund of State Key Laboratory of Precision Manufacturing for Extreme Service Performance, Central South University (Kfkt2024-06).

Data Availability Statement: No new data was created.

Conflicts of Interest: The authors declare no conflicts of interest.

References

1. Wu, Z.; Chen, D.; Li, S.; Cui, Y. Research and application progress of key technologies for composites cryogenic tanks. *Aeronautical Manufacturing Technology* **2021**, *64*, 14-23, doi: 10.16080/j.issn1671-833x.2021.11.014 (in Chinese).

 doi:10.20944/preprints202604.0440.v1

2. Reddy, S.S.P.; Suresh, R.; Hanamantraygouda., M.B.; Shivakumar, B.P. Use of composite materials and hybrid composites in wind turbine blades. *Materials Today: Proceedings* **2021**, 46, 2827-2830, doi: 10.1016/j.matpr.2021.02.745.
3. Gao, Y.; Zhao, C.Y.; Li, Y.S.; Zhu, S.; Wang, P.; Zhang, W.Z.; Wang, H. Void suppression in variable-thickness thermoplastic composites via synergistic pressure-temporal modulation and lay-up architectonics during thermoforming. *Composites Part B-Engineering* **2026**, *312*, doi: 10.1016/j.compositesb.2025.113304.
4. Wu, H.L.; Dong, H.Y.; Guo, Y.J.; Yuan, F.; Ke, Y.L. Reverse deformation design for bending control in welding of ring stiffeners. *International Journal of Pressure Vessels and Piping* **2025**, *213*, doi:10.1016/j.ijpvp.2024.105362.
5. Czerwinski, F. Current Trends in Automotive Lightweighting Strategies and Materials. *Materials* **2021**, *14*, doi:10.3390/ma14216631.
6. Ge, J.; Luo, M.; Zhang, D.H.; Catalanotti, G.; Falzon, B.G.; McClelland, J.; Higgins, C.; Jin, Y.; Sun, D. Temperature field evolution and thermal-mechanical interaction induced damage in drilling of thermoplastic CF/PEKK-A comparative study with thermoset CF/epoxy. *Journal of Manufacturing Processes* **2023**, *88*, 167-183, doi:10.1016/j.jmapro.2023.01.042.
7. He, K.; Hoa, S.V.; Ganesan, R. The study of tapered laminated composite structures: a review. *Composites Science and Technology* **2000**, *60*, 2643-2657, doi:10.1016/s0266-3538(00)00138-x.
8. Abdulhamid, H.; Bouvet, C.; Michel, L.; Aboissière, J.; Minot, C. Influence of internally dropped-off plies on the impact damage of asymmetrically tapered laminated CFRP. *Composites Part a-Applied Science and Manufacturing* **2015**, *68*, 110-120, doi:10.1016/j.compositesa.2014.09.024.
9. Liu, L.; Zhang, B.M.; Wang, D.F.; Wu, Z.J. Effects of cure cycles on void content and mechanical properties of composite laminates. *Composite Structures* **2006**, *73*, 303-309, doi:10.1016/j.compstruct.2005.02.001.
10. Ghiorse, S.R. Effect of void content on the mechanical properties of carbon/epoxy laminates. *SAMPE Quarterly* **1993**, *24*, 54-59, doi:10.1007/BF01019870.
11. Stamopoulos, A.G.; Tserpes, K.I.; Prucha, P.; Vavrik, D. Evaluation of porosity effects on the mechanical properties of carbon fiber-reinforced plastic unidirectional laminates by X-ray computed tomography and mechanical testing. *Journal of Composite Materials* **2016**, *50*, 2087-2098, doi:10.1177/0021998315602049.
12. Choudhry, R.S.; Khan, K.A.; Khan, S.Z.; Khan, M.A.; Hassan, A. Micromechanical modeling of 8-harness satin weave glass fiber-reinforced composites. *Journal of Composite Materials* **2017**, *51*, 705-720, doi:10.1177/0021998316649782.
13. Liu, H.L.; Cui, H.T.; Wen, W.D.; Su, X.M.; Kang, H.T.; Engler-Pinto, C. The effect of voids on the quasi-static tensile properties of carbon fiber/polymer-laminated composites. *Journal of Composite Materials* **2018**, *52*, 1997-2015, doi:10.1177/0021998317737827.
14. Zhu, H.Y.; Wu, B.C.; Li, D.H.; Zhang, D.X.; Chen, Y.Y. Influence of Voids on the Tensile Performance of Carbon/epoxy Fabric Laminates. *Journal of Materials Science & Technology* **2011**, *27*, 69-73, doi:10.1016/s1005-0302(11)60028-5.
15. Kosmann, N.; Karsten, J.M.; Schuett, M.; Schulte, K.; Fiedler, B. Determining the effect of voids in GFRP on the damage behaviour under compression loading using acoustic emission. *Composites Part B-Engineering* **2015**, *70*, 184-188, doi:10.1016/j.compositesb.2014.11.010.
16. Hagstrand, P.O.; Bonjour, F.; Månson, J.A.E. The influence of void content on the structural flexural performance of unidirectional glass fibre reinforced polypropylene composites. *Composites Part a-Applied Science and Manufacturing* **2005**, *36*, 705-714, doi:10.1016/j.compositesa.2004.03.007.
17. Zhang, A.Y.; Lu, H.B.; Zhang, D.X. Effects of voids on residual tensile strength after impact of hygrothermal conditioned CFRP laminates. *Composite Structures* **2013**, *95*, 322-327, doi:10.1016/j.compstruct.2012.08.001.
18. Centea, T.; Grunenfelder, L.K.; Nutt, S.R. A review of out-of-autoclave prepregs - Material properties, process phenomena, and manufacturing considerations. *Composites Part a-Applied Science and Manufacturing* **2015**, *70*, 132-154, doi:10.1016/j.compositesa.2014.09.029.
19. Ekuase, O.A.; Anjum, N.; Eze, V.O.; Okoli, O.I. A Review on the Out-of-Autoclave Process for Composite Manufacturing. *Journal of Composites Science* **2022**, *6*, doi:10.3390/jcs6060172.
20. Hubert, P.; Fernlund, G.; Poursartip, A. Autoclave processing for composites. **2012**.

 doi:10.20944/preprints202604.0440.v1

21. Hjellming, L.N.; Walker, J.S. Thermal Curing Cycles for Composite Cylinders with Thick Walls and Thermoset Resins. *Journal of Composite Materials* **1989**, *23*, 1048-1064, doi: 10.1177/002199838902301007.
22. Schechter, S.G.K.; Centea, T.; Nutt, S.R. Polymer film dewetting for fabrication of out-of-autoclave prepreg with high through-thickness permeability. *Composites Part a-Applied Science and Manufacturing* **2018**, *114*, 86-96, doi:10.1016/j.compositesa.2018.08.002.
23. Bender, D.B.; Centea, T.; Nutt, S.R. FAST CURE OF VACUUM BAG ONLY PREPREG COMPOSITES. *CAMX 2019* **2019**, doi: 10.33599/nasampe/c.19.0733.
24. Repecka, L.; Boyd, J. Vacuum-Bag-Only-Curable Prepregs That Produce Void-Free Parts. In Proceedings of the International SAMPE Symposium and Exhibition, 2002.
25. Mujahid, Y.; Sallih, N.; Abdullah, M.Z.; Mustapha, M. Effects of processing parameters for vacuum-bag-only method on void content and mechanical properties of laminated composites. *Polymer Composites* **2021**, *42*, 567-582, doi:10.1002/pc.25848.
26. Guan, C.L.; Zhan, L.H.; Sun, F.W.; Yao, S.M.; Zhong, S.C.; Wang, B. Study on the heating mechanism and macro/micro properties of composite materials under microwave curing. *Polymer Composites* **2024**, *45*, 1405-1421, doi:10.1002/pc.27862.
27. Muric-Nesic, J.; Compston, P.; Stachurski, Z.H. On the void reduction mechanisms in vibration assisted consolidation of fibre reinforced polymer composites. *Composites Part a-Applied Science and Manufacturing* **2011**, *42*, 320-327, doi:10.1016/j.compositesa.2010.12.011.
28. Zhang, D.C.; Zhan, L.H.; Ma, B.L.; Yao, S.M.; Guo, J.Z.; Guan, C.L.; Liu, S. Experimental investigation of vibration pretreatment-microwave curing process for carbon fiber reinforced resin matrix composites. *Journal of Central South University* **2024**, *31*, 1838-1855, doi:10.1007/s11771-024-5664-x.
29. Guan, C.L.; Chi, T.M.; Zhan, L.H.; Chen, J.H.; Wang, B.; Xie, L.P.; Zhong, S.C. Analysis of Deformation and Properties of Composite Melon Petals via Vibration Pretreatment-Microwave Compound Curing. *Polymers* **2023**, *15*, doi:10.3390/polym15234541.
30. Zhang, D.C.; Zhan, L.H.; Guan, C.L.; Guo, J.Z.; Ma, B.L.; Dai, G.M.; Yao, S.M. Optimization of Vibration Pretreatment Microwave Curing in Composite Laminate Molding Process. *Polymers* **2023**, *15*, doi:10.3390/polym15020296.
31. Xu, X.X.; Wei, K.; Mei, M.; Li, M.J.; Yang, X.J. An ultrasound-assisted resin transfer molding to improve the impregnation and dual-scale flow for carbon fiber reinforced resin composites. *Composites Science and Technology* **2024**, *255*, doi:10.1016/j.compscitech.2024.110710.
32. Peng, Y.F.; Li, M.J.; Yang, X.J. Void formation and suppression in CFRP laminate using newly designed ultrasonic vibration assisted RTM technique. *Composite Structures* **2024**, *329*, doi:10.1016/j.compstruct.2023.117796.
33. Meier, R.; Kahraman, I.; Seyhan, A.T.; Zaremba, S.; Drechsler, K. Evaluating vibration assisted vacuum infusion processing of hexagonal boron nitride sheet modified carbon fabric/epoxy composites in terms of interlaminar shear strength and void content. *Composites Science and Technology* **2016**, *128*, 94-103, doi:10.1016/j.compscitech.2016.03.022.
34. Biot, M.A. Theory of propagation of elastic waves in a fluid-saturated porous solid. I. Low - frequency range. *The Journal of the Acoustical Society of America* **1956**, 28(2), 168 - 78, doi: 10.1121/1.1908239.
35. Biot, M.A. Mechanics of deformation and acoustic propagation in porous media. *Journal of Applied Physics* **1962**, *33*, 1483-1498, doi: 10.1063/1.1728759.
36. Maurice; A.; Biot. Generalized Theory of Acoustic Propagation in Porous Dissipative Media. *Journal of the Acoustical Society of America* **1962**, *34, 1254-1264*, doi: 10.1121/1.1918315.